

# Contrastive Conditional Latent Diffusion for Audio-visual Segmentation

Yuxin Mao, Jing Zhang, Mochu Xiang, Yunqiu Lv, Yiran Zhong, Yuchao Dai\*

**Abstract**—We propose a latent diffusion model with contrastive learning for audio-visual segmentation (AVS) to extensively explore the contribution of audio. We interpret AVS as a conditional generation task, where audio is defined as the conditional variable for sound producer(s) segmentation. With our new interpretation, it is especially necessary to model the correlation between audio and the final segmentation map to ensure its contribution. We introduce a latent diffusion model to our framework to achieve semantic-correlated representation learning. Specifically, our diffusion model learns the conditional generation process of the ground-truth segmentation map, leading to ground-truth aware inference when we perform the denoising process at the test stage. As a conditional diffusion model, we argue it is essential to ensure that the conditional variable contributes to model output. We then introduce contrastive learning to our framework to learn audio-visual correspondence, which is proven consistent with maximizing the mutual information between model prediction and the audio data. In this way, our latent diffusion model via contrastive learning explicitly maximizes the contribution of audio for AVS. Experimental results on the benchmark dataset verify the effectiveness of our solution. Code and results are online via our project page: <https://github.com/OpenNLPLab/DiffusionAVS>.

**Index Terms**—Audio-visual segmentation, Conditional latent diffusion model, Contrastive learning.

## I. INTRODUCTION

**A**UDIO-VISUAL segmentation (AVS) aims to accurately segment the region in the image that produces the sound from the audio, which is also defined as the sound source segmentation task. Due to the usage of multimodal data, *i.e.* audio and visual, AVS is conventionally achieved via multimodal learning [1], where fusion strategies are investigated to implicitly explore the contribution of each modality. As a segmentation task, AVS is different from others, *i.e.* semantic segmentation [2] or instance segmentation [3], in that it identifies the foreground object(s) that produce the given sound in the audio, which can also be defined as a guided binary segmentation task. We argue that without audio as guidance, the visual itself in AVS is not enough to regress the AVS model. This “guided” attribute also makes AVS different from other multimodal binary segmentation, *i.e.* RGB-Depth salient object detection [4], where each unimodal data can achieve reasonable prediction. With the above understanding of AVS, we find it is essential to ensure the contribution of audio for

AVS, or the model output should be correlated with the audio. In this paper, we aim to extensively explore the contribution of audio for AVS with better data alignment modeling.

Specifically, as a conditional generation task, we aim to extensively explore the correlation of audio (the conditional variable) and the final sound producer(s) (the target), which can be achieved via maximizing the conditional log-likelihood with likelihood based generative models, *i.e.* conditional variational auto-encoders (CVAE) [5], [6], diffusion models [7], [8], *etc*CVAE [5] maximizes the likelihood via an evidence lower bound (ELBO), which is effective in general. However, it suffers from the posterior collapse issue [9] where the latent code contains nothing semantically related information. Diffusion models [10], [11] are proven more effective in producing semantic correlated latent space [12]. We then introduce the diffusion model to our AVS task to ensure semantic related information is extracted from the conditional variable. Specifically, we encode the ground-truth segmentation map and use it as the latent code, which is destroyed and generated by the diffusion model via the forward and denoising process. Further, we encode the audio-visual pair and use it as the condition, leading to a conditional generative process.

Directly using the diffusion model with conditional variables with rich semantic information can be enough to achieve conditional maximum likelihood learning. However, given the limited and less diverse training dataset [1] of our AVS task, it’s difficult to guarantee the discriminativeness of the audio based conditional variable. We want the conditional variable to be representative enough in feature space to distinguish the higher level visual semantic difference. We thus resort to contrastive learning to learn informative feature representation.

Contrastive learning [13], [14] was introduced for metric learning, and the classical contrastive loss or InfoNCE loss [15] is defined as:

$$\mathcal{L}_{\text{InfoNCE}} = \frac{1}{|\mathbf{P}|} \sum_{\mathbf{z}^+ \in \mathbf{P}} -\log \frac{\exp(s(\mathbf{z}, \mathbf{z}^+)/\tau)}{\sum_{\mathbf{z}^j \in \{\mathbf{z}^+, \mathbf{N}\}} \exp(s(\mathbf{z}, \mathbf{z}^j)/\tau)}, \quad (1)$$

which takes pair of examples ( $\mathbf{x}$  and  $\mathbf{x}'$ ) as input and trains the network to predict whether they are similar (from the same class) or dissimilar (from different classes). In Eq. (1),  $\mathbf{z}$  is the representation of the sample  $\mathbf{x}$ ,  $\mathbf{z}^+$  is the representation of the positive sample  $\mathbf{x}^+$  of  $\mathbf{x}$ ,  $\mathbf{P}$  and  $\mathbf{N}$  are the sets of positive and negative pairs corresponding to  $\mathbf{x}$ , respectively,  $s(\cdot)$  computes the dot product between  $\ell_2$  normalized feature embeddings, and  $\tau$  is the temperature, which can be learned or pre-defined.

Conventionally, contrastive learning is applied to unimodal setting [16]–[19], where data augmentation is the main strategy

Yuxin Mao, Mochu Xiang, Yunqiu Lv, Yuchao Dai are with School of Electronics and Information, Northwestern Polytechnical University, Xi’an, China.

Jing Zhang is with School of Computing, Australian National University, Canberra, Australia.

Yiran Zhong is with Shanghai AI Laboratory, China.

to construct positive/negative pairs. We are working on a special multimodal task, where contrastive learning is used to enhance the contribution or the semantic richness of the guidance (the audio data in our case). We then construct positive/negative pairs based on correspondence between the visual sound producer and the audio, where the basic idea is that the higher level semantic information of the visual sound producer and the audio should be the same, *e.g.* the category of the sound. With the leverage of contrastive learning, we aim to generate features with richer semantic information and ensure their distinction in feature space, making it suitable to serve as a conditional variable for the proposed conditional latent diffusion model. As a latent space diffusion model, the feature space reverse diffusion process restores the ground truth distribution, leading to ground-truth aware inference when we perform the denoising process at the test stage.

We summarize our main contributions as:

- We rethink AVS as a guided conditional generation task, aiming to extensively explore the semantic correlation between the guidance (the audio) and the final output (the segmentation maps).
- We introduce the latent diffusion model, and its maximum likelihood estimation objective guarantees the ground-truth aware inference.
- We adopt contrastive learning to our framework to ensure the distinction of the audio representation to achieve an effective latent diffusion model.
- Experiments show that our proposed method achieves state-of-the-art segmentation performance and extensive ablation experiments demonstrate the effectiveness of each component.

## II. RELATED WORK

**Audio-Visual Segmentation.** Audio-visual segmentation (AVS) is a challenging, newly proposed problem that predicts pixel-wise masks for the sound producer(s) in a video sequence given audio information. To tackle this issue, Zhou *et al.* [1] propose an audio-visual segmentation benchmark and provide pixel-level annotations. The dataset contains five-second videos and audio, and the binary mask is used to indicate the pixels of sounding objects for the corresponding audio. Subsequently, they proposed an encoder-decoder network based on the temporal pixel-wise audio-visual interaction as a simple baseline. However, such a feature fusion strategy considers only feature-level correlations and does not model the AVS task from its essence, *i.e.* it does not consider the guidance capability of the audio. Due to its binary segmentation nature, models for salient object detection (SOD) and video foreground segmentation (VOS) [20]–[23] (segmenting the foreground attracts human attention) are usually treated as baselines. However, the uniqueness of this task is that audio serves as guidance, leading to guided multimodal binary segmentation.

**Diffusion Models and the Applications.** The essential idea of diffusion model [7], [8], [11] is to systematically and slowly destroy the structure in a data distribution through an iterative forward diffusion process. The reverse diffusion process then

restores structures in data. [7] claims that generative models suffer from a trade-off between tractability and flexibility. A tractable model can be easily analyzed and evaluated to fit the data. A flexible model can fit structure in arbitrary data. The diffusion model allows 1) extreme flexibility in the model structure; 2) exact sampling; 3) easy multiplication with other distributions; 4) model log-likelihood and individual states can be cheaply evaluated, achieving both tractable and flexible models. DDPM [24] extends diffusion models [7] to generate high quality samples. Especially, DDPM [24] establishes a connection between diffusion models and denoising score matching, leading to a simplified, weighted variational bound objective for diffusion models. The original goal of diffusion models is to generate high quality images, making super-resolution as a straightforward application [25]. Later, diffusion models have been explored for segmentation tasks [26], [26], [27], [27], [28], [28], [28], [29], [29], [29], [30], [30], [31], [31]–[40]. Given its feature encoding nature, diffusion models have also been used for representation learning [12], [41]–[45], classification and regression [46]. Diffusion models have also been extended in 3D vision [47]. For multimodal generation [48], [49], each unimodal is treated equally, which is different from our setting that one modality serves as guidance for the conditional generation process. A comprehensive survey on diffusion models can be found at [50].

**Contrastive Learning for Representation Learning.** Contrastive loss [13], [14] was introduced for distance metric learning to decide whether the pair of data is similar or dissimilar. Taking a step further, triplet loss [51]–[53] achieves distance metric learning by using triplets, including a query sample ( $\mathbf{x}$ ), it is a positive sample ( $\mathbf{x}^+$ ) and a negative sample ( $\mathbf{x}^-$ ). The goal of triplet loss is to push the difference of similarity between positive and negative samples to the query sample to be greater than a predefined margin parameter. By pulling similar concepts to be closer in the embedding space and pushing the dissimilar ones to be far apart, triplet loss achieves better feature representation learning. However, one of the main issues is that it only learns from one negative sample, ignoring the dissimilarity with all the other candidate negative samples, leading to unbalanced metric learning. To solve this problem, [54] introduces N-pair loss to learn from multiple negative samples for balanced metric learning. SimCLR [55] produces two noise versions of  $\mathbf{x}$  via different data augmentation strategies, and it then maximizes agreement between differently augmented views of the same sample via a contrastive loss in latent space. Consider a sample  $\mathbf{x}$  and its two correlated views  $\tilde{\mathbf{x}}_i$  and  $\tilde{\mathbf{x}}_j$ , where  $\tilde{\mathbf{x}}_i$  and  $\tilde{\mathbf{x}}_j$  is defined as the positive pair, [55] design a self-supervised feature representation framework with a base encoder  $f(\cdot)$  (*e.g.* ResNet backbone) and a projection head  $g(\cdot)$  (*e.g.* a MLP), where the former is for image backbone feature extraction, and the latter produces latent space representation, where contrastive loss is applied. In this case, the contrastive prediction task aims to identify  $\tilde{\mathbf{x}}_j$  in  $\{\tilde{\mathbf{x}}_k\}_{k \neq i}$  for a given  $\tilde{\mathbf{x}}_i$ . The main strategy to achieve self-supervised contrastive learning is constructing positive/negative pairs via data augmentation techniques [16]–[19], [56]–[58]. Instead of model instance/image discrimination, dense contrastive learning [59], [60] aims to explore

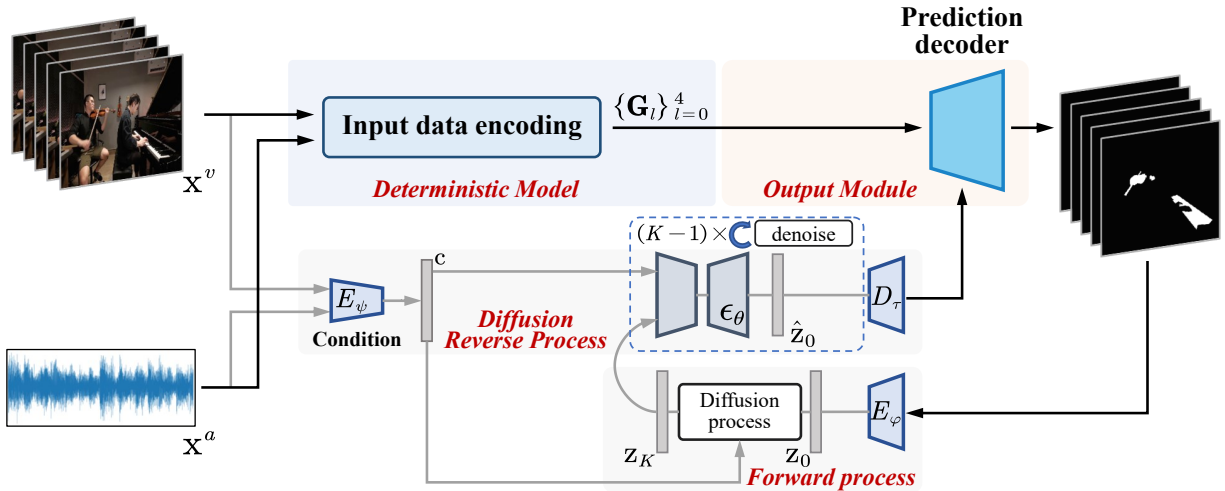


Fig. 1. **Overview of the proposed method for audio-visual segmentation.** It contains three main processes: 1) a deterministic model to perform input data encoding with deterministic features ( $\{\mathbf{G}_l\}_{l=0}^4$ ); 2) a conditional latent diffusion model to provide semantic meaningful latent representation, where contrastive learning is ignored for clear presentation. Note that the forward process with ground truth encoding ( $E_\phi$ ) is only used during training; 3) a prediction decoder to aggregate latent representation and deterministic features for output generation.

pixel-level similarity. [60] introduces pixel-wise contrastive learning, and applies it to semantic segmentation. Specifically, the positive/negative pairs, namely memory bank [55], [61]–[64], can be from the same image or different images, leading to intra/inter-image level pixel-wise contrastive learning.

### III. METHOD

Given the training dataset  $D = \{\mathbf{X}_i, \mathbf{y}_i\}_{i=1}^N$  with the input data  $\mathbf{X} = \{\mathbf{x}^v, \mathbf{x}^a\}$  ( $\mathbf{x}^v$  represents the input video with continuous frames [1],  $\mathbf{x}^a$  is the audio of the current clip) and output  $\mathbf{y}$  (the ground-truth segmentation maps of the video clip), the goal of AVS is to segment the sound producer(s) from  $\mathbf{x}^v$  with the guidance from  $\mathbf{x}^a$ .  $i$  indexes the samples, which are omitted for clear presentation. As discussed in Sec. I, AVS is unique in that audio serves as guidance to achieve guided binary segmentation, making it different from conventional multimodal learning [65], where each modal contributes nearly equally to the final output. With this understanding, we define AVS as a conditional generation task, and our goal is then to maximize the likelihood of the conditional distribution  $p(\mathbf{y}|\mathbf{x}^v, \mathbf{x}^a)$ .

A typical way to achieve this is via a variational auto-encoder (VAE) [5], [6]. However, a not well-designed VAE might suffer from the posterior collapse issue [9], where the latent variable fails to encode input related information, leading to less informative latent space. In our case, posterior collapse could lead to less extensive audio exploration. Recently, diffusion models [7], [8], [11] show potentials in many tasks, which are proven capable of achieving more semantic related latent space [12]. We thus resort to diffusion models for our AVS task (see Sec. III-A), aiming to model the distribution of  $p(\mathbf{y}|\mathbf{x}^v, \mathbf{x}^a)$ . Further, we introduce contrastive learning (see Sec. III-B) to our framework to guarantee the effectiveness of the conditional variables by explicitly modeling the correspondence between visual objects and the audio. We present

our pipeline in Sec. III-C (see Fig. 1 for an overview of the proposed method).

#### A. Conditional Latent Diffusion Model for AVS

With a conditional latent diffusion model, we aim to model the conditional distribution  $p(\mathbf{y}|\mathbf{x}^v, \mathbf{x}^a)$ , where a ground-truth related diffusion model is learned to estimate the conditional ground-truth density function, achieving ground-truth aware inference.

**Ground-Truth Latent Encoder.** We employ an encoder  $E_\phi$  to map the ground-truth segmentation map into the latent space, i.e.  $\mathbf{z}_0 = E_\phi(\mathbf{y}) \in \mathbb{R}^{B \times D}$ , where  $B$  is the batch size and  $D$  denotes the latent dimensions. Note that our ground-truth encoding process is similar to the posterior computation strategy in VAE [6]. However, the main difference is that the latent code in our case is explicitly modeled via a diffusion model, and it can follow any distributions, where the latent code in VAE is assumed to be Gaussian with the re-parameterization trick [6]. The  $E_\phi$  consists of five convolutional layers followed by leakyReLU and batch norm, and the output channels are [16, 32, 64, 64, 64], respectively. Then two fully connected layers are used to generate the latent code of size  $D = 24$ .

**Latent Conditional Diffusion Model.** Given the latent code  $\mathbf{z}_0$ , our latent conditional diffusion model aims to learn its distribution, thus we can restore the ground-truth information during testing. We first review diffusion models [7], [8]. Then, we present our conditional diffusion model to gradually diffuse  $\mathbf{z}_0$  to  $\mathbf{z}_K \sim \mathcal{N}(0, \mathbf{I})$ , and restore  $\mathbf{z}_0$  back from  $\mathbf{z}_K$  via conditional generation.

**Diffusion models** [7], [8], [11] are built upon a generative Markov chain, which converts a simple known distribution, (e.g. a Gaussian) into a target distribution (e.g. any distribution). The essential idea of diffusion model [7], [8] is to systematically and slowly destroy the structure of a sample through an iterative forward diffusion process. The reverse diffusion process then restores structures in the sample.

Following the conventional diffusion process, a latent data representation  $\mathbf{z}_0$  will be gradually converted into an analytically tractable distribution, *i.e.*  $\pi(\mathbf{z}) = \mathcal{N}(0, \mathbf{I})$ , by iteratively applying a Markov diffusion kernel  $T_\pi(\mathbf{z}|\mathbf{z}'; \beta)$  with diffusion rate  $\beta$  via:

$$q(\mathbf{z}_k|\mathbf{z}_{k-1}) = T_\pi(\mathbf{z}_k|\mathbf{z}_{k-1}; \beta_k). \quad (2)$$

The forward trajectory is thus:

$$q(\mathbf{z}_{0,\dots,K}) = q(\mathbf{z}_0) \prod_{k=1}^K q(\mathbf{z}_k|\mathbf{z}_{k-1}), \quad (3)$$

where the diffusion kernel  $q(\mathbf{z}_k|\mathbf{z}_{k-1})$  is defined as Gaussian in [7], [8] with an identity-covariance:

$$q(\mathbf{z}_k|\mathbf{z}_{k-1}) = \mathcal{N}(\mathbf{z}_k; \sqrt{1 - \beta_k} \mathbf{z}_{k-1}, \beta_k \mathbf{I}). \quad (4)$$

A notable property of the forward diffusion process is that it admits sampling  $\mathbf{z}_k$  at arbitrary timestep  $k$  in closed form:

$$q(\mathbf{z}_k|\mathbf{z}_0) = \mathcal{N}(\mathbf{z}_k; \sqrt{\bar{\alpha}_k} \mathbf{z}_0, (1 - \bar{\alpha}_k) \mathbf{I}), \quad (5)$$

where  $\alpha_k = 1 - \beta_k$  and  $\bar{\alpha}_k = \prod_{s=1}^k \alpha_s$ . Eq. (5) explains the stochastic diffusion process, where no learnable parameters are needed, and a pre-defined set of hyper-parameters, *i.e.*  $\{\beta\}_{k=1}^K$ , will lead to a set of latent variables  $\{\mathbf{z}\}_{k=1}^K$ .

The generative process or the denoising process is then to restore the sample via:

$$p_\theta(\mathbf{z}_{0,\dots,K}) = p(\mathbf{z}_K) \prod_{k=1}^K p_\theta(\mathbf{z}_{k-1}|\mathbf{z}_k), \quad (6)$$

where  $p(\mathbf{z}_K) = \pi(\mathbf{z}) = \mathcal{N}(0, \mathbf{I})$  in our case. For Gaussian diffusion, during learning, only the mean ( $\mu$ ) and variance ( $\Sigma$ ) are needed to be estimated, leading to:

$$p_\theta(\mathbf{z}_{k-1}|\mathbf{z}_k) = \mathcal{N}(\mathbf{z}_{k-1}; \mu_\theta(\mathbf{z}_k, k), \Sigma_\theta(\mathbf{z}_k, k)), \quad (7)$$

where  $\theta$  represents model parameters. In practice, [8] sets  $\Sigma$  as hyper-parameters, *i.e.*  $\Sigma_\theta(\mathbf{z}_k, k) = \beta_k \mathbf{I}$ , for stable training, thus only  $\mu_\theta(\mathbf{z}_k, k)$  is learned.

**Conditional diffusion models for AVS.** For our AVS task, with the ground-truth latent encoder  $\mathbf{z}_0 = E_\varphi(\mathbf{y})$ , Eq. (5) provides the diffusion process by gradually destroying  $\mathbf{z}_0$  to obtain  $\mathbf{z}_K \sim \mathcal{N}(0, \mathbf{I})$ . Our conditional generation process aims to restore  $\mathbf{z}_0$  given the input data  $\mathbf{c} = E_\psi(\mathbf{x}^v, \mathbf{x}^a)$ , where  $\mathbf{c}$  is the feature embedding of our input, leading to the conditional generative process  $p_\theta(\mathbf{z}_{k-1}|\mathbf{z}_k, \mathbf{c})$  (Although we aim to correlate output with audio, as no appearance information is presented in the binary ground truth, we take the fused feature  $\mathbf{c}$  instead of the audio feature to correlate “visual” sound producer(s) with the audio data). We thus sample from  $p_\theta(\mathbf{z}_0|\mathbf{c})$  via:

$$p_\theta(\mathbf{z}_0|\mathbf{c}) = \int p_\theta(\mathbf{z}_{0,\dots,K}|\mathbf{c}) d\mathbf{z}_{1,\dots,K}, \quad (8)$$

$$p_\theta(\mathbf{z}_{0,\dots,K}|\mathbf{c}) = p(\mathbf{z}_K) \prod_{k=1}^K p_\theta(\mathbf{z}_{k-1}|\mathbf{z}_k, \mathbf{c}).$$

Following the simplified diffusion model objective [8], with the re-parameterization trick [6], a noise estimator  $\epsilon_\theta$  is designed to regress the actual noise  $\epsilon$  added to  $\mathbf{z}_k$  via:

$$\mathcal{L}_{\text{simple}}(\theta) := \mathbb{E}_{\mathbf{z}, \mathbf{c}, \epsilon \sim \mathcal{N}(0, \mathbf{I}), k} \left[ \|\epsilon - \epsilon_\theta(\mathbf{z}_k, \mathbf{c}, k)\|^2 \right]. \quad (9)$$

At inference time, given feature  $\mathbf{c}$  of the audio-visual pair and random noise  $\mathbf{z}_K \sim \mathcal{N}(0, \mathbf{I})$ , our model samples  $p_\theta(\mathbf{z}_0|\mathbf{c})$  via Eq. (8) by gradually performing denoising.

**Technical details.** Following the conventional practice in designing the diffusion models [8], the noise estimator  $\epsilon_\theta$  in our case is a UNet structure, which consists of eight fully connected layers followed by leakyReLU activation, the former four layers are “encoder” and the latter four layers are “decoder”.

The effectiveness of  $p_\theta(\mathbf{z}_0|\mathbf{c})$  depends on the representativeness of the conditional variable  $\mathbf{c}$ , which can be addressed by contrastive learning [13]–[15], [51]–[55].

### B. Contrastive Representation Learning

As a conditional generation model, we argue that the representativeness of the conditional variable(s) plays an important role in the sample quality, especially for our specific multimodal task, where audio data serves as guidance for the visual data to achieve guided segmentation. We will first introduce our conditional variable generation process, *i.e.*  $\mathbf{c} = E_\psi(\mathbf{x}^v, \mathbf{x}^a)$ , and then present our positive/negative pairs construction for contrastive learning.

**Generating the Conditional Feature  $\mathbf{c}$ .** We encode visual-audio pairs into the conditional latent code  $\mathbf{c}$ . Specifically,  $E_\psi$  can be divided into two branches, namely the visual branch and the audio branch. The visual branch consists of five convolutional layers and two fully connected layers, which share the same structure of  $E_\varphi$ . The audio branch involves two fully connected layers. Further, the visual features and the audio features are concatenated channel-wisely and another two fully connected layers are used to get the final conditional embedding  $\mathbf{c}$ .

**Positive/Negative Pair Construction.** One of the key challenges of contrastive learning is positive/negative pairs construction, based on which metric learning [66] can be achieved. Metric learning [66] is the proper choice to automate the distance function selection process, aiming to learn task-specific distance functions in a supervised manner. For our AVS task, we aim to learn a suitable distance function, thus the paired audio/visual sound producer(s) data should stay closer in feature space than the unpaired ones.

Besides the latent code  $\mathbf{z}_0$ , we have three variables involved in our framework, namely video  $\mathbf{x}^v$ , audio  $\mathbf{x}^a$ , and ground-truth segmentation map  $\mathbf{y}$ . As discussed in Sec. III-A, we design a diffusion model to diffuse and restore the ground-truth information, thus we can sample from  $p_\theta(\mathbf{z}_0|\mathbf{c})$  via Eq. (8). In that case, we claim that the conditional variable  $\mathbf{c}$  should be discriminative enough to distinguish  $\mathbf{z}_0$ . In other words, given  $\mathbf{c}$ , the corresponding  $\mathbf{z}_0$  should lead to a larger score than  $\mathbf{z}'_0$  of another sound producer(s). Specifically, with audio-visual feature  $\mathbf{c} = E_\psi(\mathbf{x}_i^v, \mathbf{x}_i^a)$ , we define its ground-truth encoding  $\mathbf{z}_0 = E_\varphi(\mathbf{y}_i)$  as its positive sample, and  $\mathbf{y}'$  other than  $\mathbf{y}_i$  in the mini-batch as the negative samples. With the above positive/negative samples, we obtain our contrastive loss as:

$$\mathcal{L}_{\text{contrastive}}(\psi) = -\mathbb{E}_{\mathbf{z}_0} \left[ \log \frac{f(\mathbf{z}_0, \mathbf{c})/\tau}{\sum_{\mathbf{z}'_0 \in \{\mathbf{N}, \mathbf{z}_0\}} f(\mathbf{z}'_0, \mathbf{c})/\tau} \right], \quad (10)$$

where  $\mathbf{z}_0$  is always paired with  $\mathbf{c}$ , and  $\mathbf{N}$  represents the negative samples within the mini-batch, which includes all the samples except  $\mathbf{z}_0$ ,  $f(\mathbf{z}_0, \mathbf{c}) = \exp(s(\mathbf{z}_0, \mathbf{c}))$  (see Eq. (1)) estimates the density ratio  $\frac{p(\mathbf{z}_0|\mathbf{c})}{p(\mathbf{z}_0)}$ .  $\tau$  is a temperature parameter and we set  $\tau=1$  in all experiments.

**Mutual Information Maximization Analysis.** Mutual Information (MI) captures the nonlinear statistical dependencies between variables. Specifically, for random variables  $\mathbf{z}_0$  and  $\mathbf{c}$ , their mutual information is defined as:

$$\begin{aligned} I(\mathbf{z}_0; \mathbf{c}) &= \sum_{\mathbf{z}_0, \mathbf{c}} p(\mathbf{z}_0, \mathbf{c}) \log \frac{p(\mathbf{z}_0, \mathbf{c})}{p(\mathbf{z}_0)p(\mathbf{c})} \\ &= \sum_{\mathbf{z}_0, \mathbf{c}} p(\mathbf{z}_0, \mathbf{c}) \log \frac{p(\mathbf{z}_0|\mathbf{c})}{p(\mathbf{z}_0)} \propto \sum_{\mathbf{z}_0, \mathbf{c}} p(\mathbf{z}_0, \mathbf{c}) \log f(\mathbf{z}_0, \mathbf{c}). \end{aligned} \quad (11)$$

With the contrastive loss in Eq. (10), we aim to maximize the density ratio  $f(\mathbf{z}_0, \mathbf{c})$ , which in turn can be explained as achieving mutual information maximization between  $\mathbf{z}_0$  and  $\mathbf{c}$ , thus our contrastive loss explicitly explores the contribution of  $\mathbf{c}$  for the segmentation representation  $\mathbf{z}_0$ .

### C. Model Prediction Generation and Training

In Sec. III-A we present our conditional latent diffusion model to learn a conditional distribution  $p_\theta(\mathbf{z}_0|\mathbf{c})$ , restoring the ground truth information  $\hat{\mathbf{z}}_0$  during inference, where the discriminativeness of the conditional variable and its contribution to the final output is constrained via the contrastive learning pipeline (see Sec. III-B). As shown in Fig. 1, the restored  $\hat{\mathbf{z}}_0$  and the input data encoding are feed to the prediction decoder to generate our final prediction.

**Input Data Encoding.** We design an Audio-Visual network to produce a set of multi-scale deterministic feature maps from the input audio-visual pairs. Similar to AVSBench [1], we encode the audio and visual features from two branches. For the audio branch, we first process the audio waveform to a spectrogram via the short-time Fourier transform, and then fed it to the frozen VGGish [67] model, which is an audio classification network and per-trained on AudioSet [68]. We denote the audio features as  $\mathbf{A} \in \mathbb{R}^{T \times d}$ , where  $d = 128$  is the feature dimension. Given the video sequence  $\mathbf{x}^v$ , we encode visual features from ImageNet pre-trained ResNet50 [69] (or PVTv2 [70]) backbone. Finally, we obtain the multi-scale visual features as  $\mathbf{F}_l \in \mathbb{R}^{T \times c_l \times h_l \times w_l}$ , where  $c_l$  indicates the channel numbers and  $(h_l, w_l) = (H, W)/2^{l+1}$ .  $(H, W)$  is the spatial size of the input video and  $l \in [1, 4]$  represents the feature levels. For the ResNet50 backbone, the channel sizes of the four stages are  $c_{1:4} = [256, 512, 1024, 2048]$ . And for the PVTv2 backbone,  $c_{1:4} = [64, 128, 320, 512]$ . Additionally, we use four convolutional layers to further post-process the visual features  $\mathbf{F}_l$  to  $\mathbf{V}_l \in \mathbb{R}^{T \times c \times h_l \times w_l}$ , where  $c = 128$ . Further, given the audio-visual features, namely  $\mathbf{A}$  and  $\mathbf{V}_l$ , we exploit the temporal pixel-wise audio-visual interaction module [1] to perform audio-visual fusion in the feature space, which is a cross modal attention module to explore the audio-visual feature correlation. Finally, we obtain the deterministic feature maps  $\mathbf{G}_l \in \mathbb{R}^{T \times c \times h_l \times w_l}$ , which contains audio-visual information.

**Prediction decoder.** Since the deterministic features  $\mathbf{G}_l$  and stochastic representation  $\hat{\mathbf{z}}_0$  are with different feature sizes, to fuse the two items, we perform a latent code expanding module  $D_\tau$ , which contains one  $3 \times 3$  convolutional layer, to achieve feature expanding of  $\hat{\mathbf{z}}_0$ . Specifically, we first expand  $\hat{\mathbf{z}}_0$  to a 2D tensor and tile it to the same spatial size as  $\mathbf{G}_4$ . We define the new 2D feature map as  $\hat{\mathbf{z}}_0^e$ . Given that the spatial size of  $\hat{\mathbf{z}}_0^e$  and  $\mathbf{G}_4$  are the same, we perform cascaded channel-wise feature concatenation and one  $3 \times 3$  convolution to obtain  $\hat{\mathbf{G}}_4$ , which is the same size as  $\mathbf{G}_4$ . We use the decoder of Panoptic-FPN [71] to decode the mixed features  $\{\{\mathbf{G}_l\}_{l=1}^3, \hat{\mathbf{G}}_4\}$ . The final output of the decoder is  $\mathbf{M} \in \mathbb{R}^{T \times 1 \times H \times W}$  and activated by a sigmoid function.

**Objective function.** As a segmentation task, our model is trained with a cross-entropy loss with the ground-truth segmentation map as supervision. We also have a conditional diffusion module and a contrastive learning pipeline involved, leading to our final objective as:

$$\mathcal{L} = \mathcal{L}_{\text{seg}} + \lambda_1 \mathcal{L}_{\text{simple}} + \lambda_2 \mathcal{L}_{\text{contrastive}}, \quad (12)$$

where  $\lambda_1$  and  $\lambda_2$  are used to balance the two objectives, which are set empirically as 1 and 0.1, respectively.

## IV. EXPERIMENTAL RESULTS

### A. Setup

**Datasets.** We use the AVSBench [1], a dataset with 5,356 audio-video pairs and pixel-wise annotations to perform our experiments. Each audio-video pair in the dataset is 5 seconds and the video is trimmed to five consecutive frames by extracting the video frame at the end of each second. The AVSBench is divided into semi-supervised Single Sound Source Segmentation (S4) with only the first frame labeled, and fully supervised Multiple Sound Source Segmentation (MS3) with all frames labeled. And there are 4,922 videos in the S4 subset, and 424 videos in the MS3 subset. We train our model on the training set and perform evaluations on the testing set.

**Evaluation Metrics.** Being the same as AVSBench [1], we evaluate the audio-visual segmentation performance by using Mean Intersection over Union (mIoU) and F-score. The F-score is defined as:  $F_\beta = \frac{(1+\beta^2) \times \text{precision} \times \text{recall}}{\beta^2 \times \text{precision} + \text{recall}}$ ,  $\beta^2 = 0.3$ , where both precision and recall are based on binary segmentation map (with 256 uniformly distributed binarization thresholds in the range of  $[0, 255]$ ).

**Compared Methods.** We compare our method with AVSBench [1], and other related segmentation tasks, such as video foreground segmentation models (VOS) [20], [21], RGB image based salient object detection models [22], [23], which is strictly in accordance with the settings in previous work [1]. We set up the comparison due to the binary video segmentation nature of AVS. Being consistent with AVSBench, we also use two backbones, ResNet50 [69] and PVT [70] initialized with ImageNet [72] pre-trained weights, to demonstrate the effectiveness of our solution.

**Implementation.** Our proposed method is trained end-to-end using the Adam optimizer [73] with default hyper-parameters for 15 and 30 epochs on the S4 and MS3 subsets. The learning

TABLE I  
 QUANTITATIVE COMPARISON AGAINST RELATED MODELS ON THE S4 AND MS3 SUBSETS IN TERMS OF mIOU AND F-SCORE. WE USE TWO BACKBONES (“R50” AND “PVT”) TO DEMONSTRATE THAT OUR METHOD ACHIEVES A CONSISTENT PERFORMANCE IMPROVEMENT.

Setting	Metric	VOS		SOD		AVS			
		3DC [20]	SST [21]	iGAN [23]	LGVT [22]	AVSBench (R50) [1]	AVSBench (PVT) [1]	Ours (R50)	<b>Ours (PVT)</b>
S4	mIoU	57.10	66.29	61.59	74.94	72.79	78.74	75.80	<b>81.38</b>
	F-score	0.759	0.801	0.778	0.873	0.848	0.879	0.869	<b>0.902</b>
MS3	mIoU	36.92	42.57	42.89	40.71	47.88	54.00	49.77	<b>58.18</b>
	F-score	0.503	0.572	0.544	0.593	0.578	0.645	0.621	<b>0.709</b>

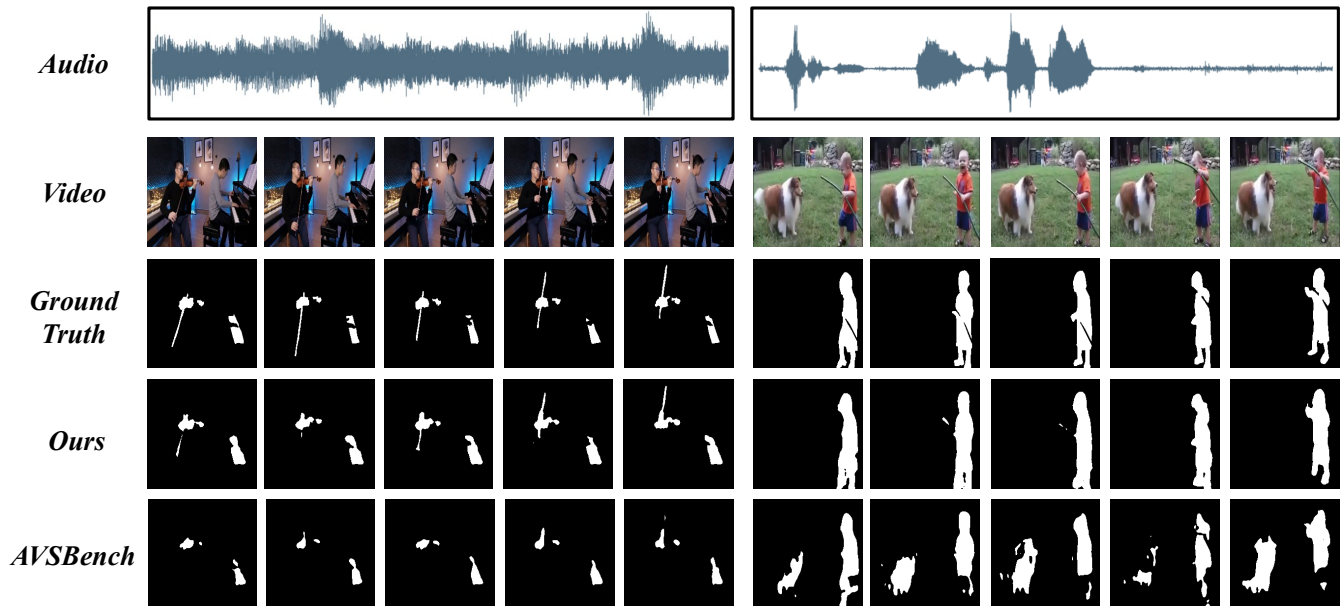


Fig. 2. **Qualitative comparison with existing method** under the fully-supervised MS3 setting. Our proposed method produces much more accurate and high-quality segmentation maps and provides a more accurate sound source localization performance.

rate is set to  $10^{-4}$  and the batch size is 4. All the video frames are resized to the shape of  $224 \times 224$ . For the latent diffusion model, we use the cosine noise schedule and the noise prediction objective in Eq. (9) for all experiments. The diffusion steps  $K$  is set as 20. To accelerate sampling, we use the DDIM [74] with 10 sampling steps.

**B. Performance Comparison**

**Quantitative Comparison.** The quantitative results on the test set of S4 and MS3 are presented in Table I. We can observe that our method consistently achieves better performance on MS3 and S4 subsets in terms of mIoU and F-score, outperforming state-of-the-art AVS methods by a large margin. There is a consistent performance improvement of our proposed method compared to AVSBench, regardless of whether “R50” or “PVT” is used as the backbone. Particularly, 4.18 and 2.58 higher mIoU than AVSBench [1] is obtained on the two subsets with “PVT” backbone. It is worth noting that our “R50” based model slightly outperforms the LGVT [22] under the S4 subset, despite LGVT using a swin transformer [75] backbone, while AVSBench (R50) performs worse than LGVT. This

suggests that exploring matching relationships between visual objects and sounds is more important than using a better visual backbone for AVS tasks. Note that the performance improvement benefits from the effective latent diffusion with the contrastive loss design itself, but does not come from more trainable parameters. Because the  $E_\varphi$ ,  $E_\psi$ ,  $D_\tau$ , and  $\epsilon_\theta$  are lightweight enough with total 4M parameters, thus the capacity of our model is comparable with AVSBench.

**Qualitative Comparison.** In Fig. 2, we show the qualitative comparison of our method with the existing method, namely AVSBench [1]. Our method tends to output segmentation results with finer details, *i.e.* an accurate segmentation of the *bow of the violin* and the *piano-key* in the left sample in Fig. 2. Additionally, our method also has the ability to identify the true sound producer, such as the *boy* in the right sample in Fig. 2, indicating a better sound localization performance. While [1] segments the two foreground objects, ignoring the audio information as guidance.

TABLE II  
**ABLATION ON THE LATENT DIFFUSION MODEL.** “E-D” INDICATES THE DETERMINISTIC ENCODER-DECODER STRUCTURE. “CVAE” DENOTES USING CVAE TO GENERATE THE LATENT CODE. “LDM” IS OUR PROPOSED LATENT DIFFUSION MODEL

Methods	S4		MS3	
	mIoU	F-score	mIoU	F-score
E-D	78.89	0.881	54.28	0.648
CVAE	79.97	0.888	55.21	0.661
LDM (Ours)	<b>81.02</b>	<b>0.894</b>	<b>57.67</b>	<b>0.698</b>

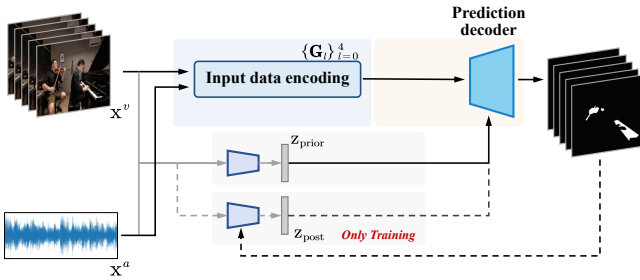


Fig. 3. **Overview of the CVAE for audio-visual segmentation**, where the posterior latent code is only used in training.

### C. Experimental Analysis

**Ablation on Latent Diffusion Model.** As discussed in the introduction section (Sec. I), a likelihood conditional generative model exactly fits our current conditional generation setting, thus a conditional variational auto-encoder [5], [6] can be a straightforward solution. To verify the effectiveness of our latent diffusion model, we design two baselines and show the comparison results in Table II. Firstly, we design a deterministic model with a simple encoder-decoder structure (“E-D”), where the input data encoding  $\{G_t\}_{t=1}^4$  is feed directly to the prediction decoder (see Fig. 1). Note that “E-D” is the same as AVSBench [1], and we retrain it in our framework and get similar performance as the original numbers reported in their paper. Secondly, to explain the superiority of the diffusion model compared with other likelihood based generative models, namely conditional variational auto-encoder [5] in our scenario, we follow [4] and design an AVS model based on CVAE (“CVAE”). CVAE [5] was introduced to RGB-Depth salient object detection in [4], where early fusion is used for latent feature encoding. We follow a similar pipeline and perform latent feature encoding based on the fused feature  $\{G_t\}_{t=0}^4$  instead of the early fusion feature due to our audio-visual setting, which is different from the visual-visual setting in [4]. Specifically, the CVAE [5] pipeline for our AVS task consists of an inference process and a generative process, where the inference process infers the latent variable  $z$  by  $p_\theta(z|X)$ , and the generative process produces the output via  $p_\theta(y|X, z)$ . The full pipeline of the CVAE for the audio-visual segmentation task can be shown in Fig. 3.

Results in Table II show that generative models can improve the performance of AVS by providing more meaningful latent space compared with the deterministic models. Further, the

TABLE III  
**ABLATION ON THE CONDITIONAL VARIABLE**, WHERE WE REMOVE IT (“NONE”), OR REPLACE IT WITH AUDIO OR VISUAL REPRESENTATION.

Methods	S4		MS3	
	mIoU	F-score	mIoU	F-score
None	80.04	0.889	56.12	0.671
Audio	80.29	0.892	56.59	0.680
Visual	80.68	0.892	57.21	0.688
audio-visual (Ours)	<b>81.02</b>	<b>0.894</b>	<b>57.67</b>	<b>0.698</b>

TABLE IV  
**ABLATION OF CONTRASTIVE LEARNING.** WE PERFORM EXPERIMENTS WITHOUT THE  $\mathcal{L}_{\text{CONTRASTIVE}}$  TO SHOW ITS EFFECTIVENESS.

Methods	S4		MS3	
	mIoU	F-score	mIoU	F-score
w/o $\mathcal{L}_{\text{contrastive}}$	81.02	0.894	57.67	0.698
w $\mathcal{L}_{\text{contrastive}}$	<b>81.38</b>	<b>0.902</b>	<b>58.18</b>	<b>0.709</b>

latent diffusion model provides a more powerful latent space modeling capability than our implemented CVAE counterpart. Note that, as no latent code is involved in “E-D”, we do not perform contrastive learning. For a fair comparison, the contrastive learning objective  $\mathcal{L}_{\text{contrastive}}$  is not involved in “CVAE” or “LDM (Ours)” either.

**Ablation on Audio-Visual Condition.** To further understand the effectiveness of the audio-visual conditioning in the training process of the latent diffusion model, we train three models with different conditional variables  $c$ , and show performance in Table III. Firstly, we remove the conditional variable, leading to unconditional generation  $p_\theta(z_{k-1}|z_k)$ , and show the performance as “None”. Then we define unimodal audio or visual as only one conditional variable. To achieve this, we simply use the feature of each individual model before multimodal feature concatenation (see  $E_\psi$  in Sec.III-B), leading to audio/visual as conditional variable based models, namely “Audio” and “Visual” in Table III. Compared with the unconditional generation, the conditional generation can bring performance gains, and the best performance can be obtained by using the audio-visual condition. We can also observe that the performance of taking the visual data as conditioning is better than taking audio as the conditional variable. We believe this can be explained from two main aspects. Firstly, our dataset is small and less diverse, leading to less effective audio information exploration as we pretrained our model on a large visual image dataset. Secondly, the audio encoder is smaller compared with the visual encoder. More investigation will be conducted to balance the data distribution. Similar to ablation on latent diffusion model, we do not perform contrastive learning in those related experiments in Table III for a fair comparison.

**Ablation on Contrastive Learning.** We introduce contrastive learning to our framework to learn the discriminative conditional variable  $c$ . We then train our model directly without contrastive learning and show its performance as “w/o  $\mathcal{L}_{\text{contrastive}}$ ” in Table IV, where “w  $\mathcal{L}_{\text{contrastive}}$ ” is our final performance in

TABLE V  
PERFORMANCE COMPARISON WITH DIFFERENT INITIALIZATION STRATEGIES (TRAIN FROM SCRATCH OR PRE-TRAIN ON S4) UNDER MS3 SETTING IN TERMS OF mIoU. WE USE THE ARROWS WITH SPECIFIC VALUES TO INDICATE THE PERFORMANCE GAIN.

Methods	From scratch		Pre-trained on S4
AVSBench (R50) [1]	47.88	+6.45 →	54.33
AVSBench (PVT) [1]	54.00	+3.34 →	57.34
Ours (R50)	<b>49.77</b>	+7.82 →	<b>57.59</b>
Ours (PVT)	<b>58.18</b>	+2.76 →	<b>60.94</b>

Table I. The improved performance of “w  $\mathcal{L}_{\text{contrastive}}$ ” indicates the effectiveness of contrastive learning in our framework. Apart from that, we find contrastive learning works poorly with the naive encoder-decoder framework, especially with our limited computation configuration, where we cannot construct large enough positive/negative pools. However, we find the improvement is not significant compared with using contrastive learning in other tasks [76]. We argue the main reason is that our dataset is less diverse to learn distinctive enough features. We will investigate self-supervised learning to further explore contrastive learning in our framework.

**Analysis of the Per-training Strategy.** As discussed in [1], we also train our model with the full parameters initialized by the weight per-trained on the S4 subset. The performance comparison is shown in Table V. It is verified that the pre-training strategy is beneficial in all the settings with our proposed method, using “R50” or “PVT” as a backbone.

**Ablation on Size of The Latent Space:** We perform extra ablation on the size of the latent space. In the main experiment, after parameter tuning, we find  $D = 24$  works best. Here, we conduct experiments with different latent sizes, and show performance in Table VI. An obvious observation is that the size of the latent space should not be too large ( $D = 32$ ) for the diffusion model, which can have significant performance degradation, and we obtain relative stable predictions with the latent code dimension in the range of  $D \in [16, 24]$ .

TABLE VI  
ABLATION ON THE SIZE OF THE LATENT SPACE, WHERE WE CONDUCT EXPERIMENTS WITH DIFFERENT LATENT SIZES.

Latent Size	S4		MS3	
	mIoU	F-score	mIoU	F-score
$D = 8$	81.04	0.892	57.28	0.689
$D = 16$	81.18	0.895	57.98	0.704
$D = 24$	<b>81.38</b>	<b>0.902</b>	<b>58.18</b>	<b>0.709</b>
$D = 32$	80.78	0.891	57.01	0.687

**Failure Case Analysis:** We perform failure case analysis on our proposed method and the AVSBench [1]. As shown in Fig. 4, both ours and AVSBench can not deal with the absenting of segmented objects due to sound interruptions. This is due to the fact that neither we nor AVSBench took into account the “timing discontinuity” of the sound in the modeling process. However, our proposed method is still able to provide a high-quality sound source localization result.

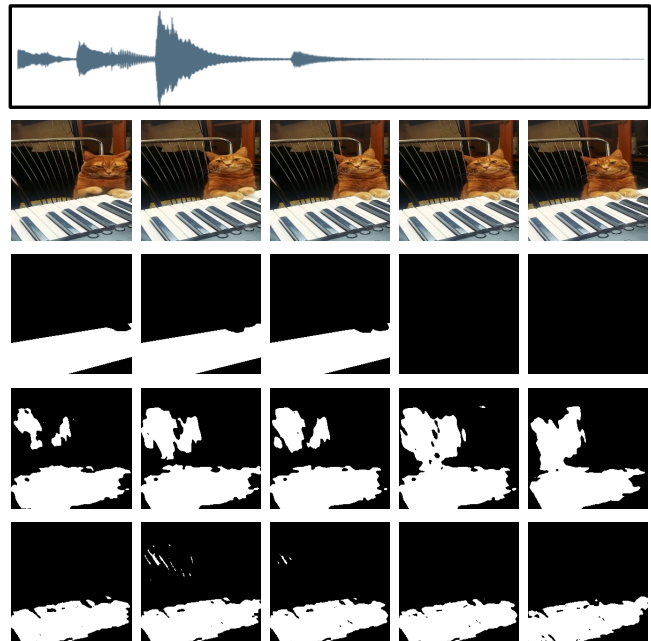


Fig. 4. Failure case on the fully-supervised MS3 setting.

## V. CONCLUSION

We have proposed a conditional latent diffusion model with contrastive learning for audio-visual segmentation (AVS). We first define AVS as a guided binary segmentation task, where audio serves as the guidance for sound producer(s) segmentation. Based on the conditional setting, we have introduced a conditional latent diffusion model to maximize the conditional log-likelihood, where the diffusion model is chosen to produce semantic correlated latent space. Specifically, our latent diffusion model learns the conditional ground truth feature generation process, and the reverse diffusion process can then restore the ground-truth information during inference. Contrastive learning has been studied to further enhance the discriminativeness of the conditional variable, leading to mutual information maximization between the conditional variable and the final output. Quantitative and qualitative evaluations on the AVSBench dataset verify the effectiveness of our solution.

## REFERENCES

- [1] J. Zhou, J. Wang, J. Zhang, W. Sun, J. Zhang, S. Birchfield, D. Guo, L. Kong, M. Wang, and Y. Zhong, “Audio-visual segmentation,” in *Proceedings of the European Conference on Computer Vision (ECCV)*, 2022, pp. 386–403. 1, 2, 3, 5, 6, 7, 8
- [2] L.-C. Chen, G. Papandreou, I. Kokkinos, K. Murphy, and A. L. Yuille, “Deeplab: Semantic image segmentation with deep convolutional nets, atrous convolution, and fully connected crfs,” *IEEE Transactions on Pattern Analysis and Machine Intelligence (T-PAMI)*, vol. 40, no. 4, pp. 834–848, 2017. 1
- [3] K. He, G. Gkioxari, P. Dollár, and R. Girshick, “Mask r-cnn,” in *Proceedings of the IEEE International Conference on Computer Vision (ICCV)*, 2017, pp. 2961–2969. 1
- [4] J. Zhang, D.-P. Fan, Y. Dai, S. Anwar, F. S. Saleh, T. Zhang, and N. Barnes, “Uc-net: Uncertainty inspired rgb-d saliency detection via conditional variational autoencoders,” in *Proceedings of the IEEE Conference on Computer Vision and Pattern Recognition (CVPR)*, 2020, pp. 8582 – 8591. 1, 7



- [5] K. Sohn, H. Lee, and X. Yan, “Learning structured output representation using deep conditional generative models,” in *Proceedings of the Advances in Neural Information Processing Systems (NeurIPS)*, 2015, pp. 3483–3491. [1](#), [3](#), [7](#)
- [6] D. P. Kingma and M. Welling, “Auto-encoding variational bayes,” in *Proceedings of the The International Conference on Learning Representations (ICLR)*, 2014. [1](#), [3](#), [4](#), [7](#)
- [7] J. Sohl-Dickstein, E. A. Weiss, N. Maheswaranathan, and S. Ganguli, “Deep unsupervised learning using nonequilibrium thermodynamics,” in *International Conference on Machine Learning (ICML)*, 2015, pp. 2256–2265. [1](#), [2](#), [3](#), [4](#)
- [8] J. Ho, A. Jain, and P. Abbeel, “Denoising diffusion probabilistic models,” *Proceedings of the Advances in Neural Information Processing Systems (NeurIPS)*, pp. 6840–6851, 2020. [1](#), [2](#), [3](#), [4](#)
- [9] J. Lucas, G. Tucker, R. Grosse, and M. Norouzi, “Understanding posterior collapse in generative latent variable models,” in *Proceedings of the The International Conference on Learning Representations Workshop (ICLRW)*, 2019. [1](#), [3](#)
- [10] A. Vahdat, K. Kreis, and J. Kautz, “Score-based generative modeling in latent space,” in *Proceedings of the Advances in Neural Information Processing Systems (NeurIPS)*, 2021, pp. 11 287–11 302. [1](#)
- [11] Y. Song, J. Sohl-Dickstein, D. P. Kingma, A. Kumar, S. Ermon, and B. Poole, “Score-based generative modeling through stochastic differential equations,” in *Proceedings of the The International Conference on Learning Representations (ICLR)*, 2021. [1](#), [2](#), [3](#)
- [12] D. Baranchuk, I. Rubachev, A. Voynov, V. Khruikov, and A. Babenko, “Label-efficient semantic segmentation with diffusion models,” in *Proceedings of the The International Conference on Learning Representations (ICLR)*, 2022. [1](#), [2](#), [3](#)
- [13] S. Chopra, R. Hadsell, and Y. LeCun, “Learning a similarity metric discriminatively, with application to face verification,” in *Proceedings of the IEEE Conference on Computer Vision and Pattern Recognition (CVPR)*, 2005, pp. 539–546. [1](#), [2](#), [4](#)
- [14] R. Hadsell, S. Chopra, and Y. LeCun, “Dimensionality reduction by learning an invariant mapping,” in *Proceedings of the IEEE Conference on Computer Vision and Pattern Recognition (CVPR)*, 2006, pp. 1735–1742. [1](#), [2](#), [4](#)
- [15] A. v. d. Oord, Y. Li, and O. Vinyals, “Representation learning with contrastive predictive coding,” *arXiv preprint arXiv:1807.03748*, 2018. [1](#), [4](#)
- [16] X. Wang, R. Zhang, C. Shen, T. Kong, and L. Li, “Dense contrastive learning for self-supervised visual pre-training,” in *Proceedings of the IEEE Conference on Computer Vision and Pattern Recognition (CVPR)*, 2021, pp. 3024–3033. [1](#), [2](#)
- [17] P. O. O Pinheiro, A. Almahairi, R. Benmalek, F. Golemo, and A. C. Courville, “Unsupervised learning of dense visual representations,” *Proceedings of the Advances in Neural Information Processing Systems (NeurIPS)*, pp. 4489–4500, 2020. [1](#), [2](#)
- [18] K. Chaitanya, E. Erdil, N. Karani, and E. Konukoglu, “Contrastive learning of global and local features for medical image segmentation with limited annotations,” *Proceedings of the Advances in Neural Information Processing Systems (NeurIPS)*, pp. 12 546–12 558, 2020. [1](#), [2](#)
- [19] E. Xie, J. Ding, W. Wang, X. Zhan, H. Xu, P. Sun, Z. Li, and P. Luo, “Detco: Unsupervised contrastive learning for object detection,” in *Proceedings of the IEEE International Conference on Computer Vision (ICCV)*, 2021, pp. 8392–8401. [1](#), [2](#)
- [20] S. Mahadevan, A. Athar, A. Ošep, S. Hennen, L. Leal-Taixé, and B. Leibe, “Making a case for 3d convolutions for object segmentation in videos,” *arXiv preprint arXiv:2008.11516*, 2020. [2](#), [5](#), [6](#)
- [21] B. Duke, A. Ahmed, C. Wolf, P. Aarabi, and G. W. Taylor, “Sstvos: Sparse spatiotemporal transformers for video object segmentation,” in *Proceedings of the IEEE Conference on Computer Vision and Pattern Recognition (CVPR)*, 2021, pp. 5912–5921. [2](#), [5](#), [6](#)
- [22] J. Zhang, J. Xie, N. Barnes, and P. Li, “Learning generative vision transformer with energy-based latent space for saliency prediction,” *Proceedings of the Advances in Neural Information Processing Systems (NeurIPS)*, pp. 15 448–15 463, 2021. [2](#), [5](#), [6](#)
- [23] Y. Mao, J. Zhang, Z. Wan, Y. Dai, A. Li, Y. Lv, X. Tian, D.-P. Fan, and N. Barnes, “Transformer transforms salient object detection and camouflaged object detection,” *arXiv preprint arXiv:2104.10127*, 2021. [2](#), [5](#), [6](#)
- [24] J. Ho, A. Jain, and P. Abbeel, “Denoising diffusion probabilistic models,” in *Proceedings of the Advances in Neural Information Processing Systems (NeurIPS)*, 2020. [2](#)
- [25] C. Saharia, J. Ho, W. Chan, T. Salimans, D. J. Fleet, and M. Norouzi, “Image super-resolution via iterative refinement,” *IEEE Transactions on Pattern Analysis and Machine Intelligence (T-PAMI)*, 2022. [2](#)
- [26] D. Baranchuk, I. Rubachev, A. Voynov, V. Khruikov, and A. Babenko, “Label-efficient semantic segmentation with diffusion models,” in *Proceedings of the The International Conference on Learning Representations (ICLR)*, 2022. [2](#)
- [27] E. A. Bremping, S. Kornblith, T. Chen, N. Parmar, M. Minderer, and M. Norouzi, “Denoising pretraining for semantic segmentation,” in *Proceedings of the IEEE Conference on Computer Vision and Pattern Recognition (CVPR)*, 2022, pp. 4175–4186. [2](#)
- [28] J. Wolleb, R. Sandkühler, F. Bieder, P. Valmaggia, and P. C. Cattin, “Diffusion models for implicit image segmentation ensembles,” in *International Conference on Medical Imaging with Deep Learning*, 2022, pp. 1336–1348. [2](#)
- [29] T. Chen, L. Li, S. Saxena, G. Hinton, and D. J. Fleet, “A generalist framework for panoptic segmentation of images and videos,” *arXiv preprint arXiv:2210.06366*, 2022. [2](#)
- [30] X. Chen, Z. Zhao, F. Yu, Y. Zhang, and M. Duan, “Conditional diffusion for interactive segmentation,” in *Proceedings of the IEEE International Conference on Computer Vision (ICCV)*, 2021, pp. 7325–7334. [2](#)
- [31] T. Amit, E. Nachmani, T. Shaharabany, and L. Wolf, “Segdiff: Image segmentation with diffusion probabilistic models,” *arXiv preprint arXiv:2112.00390*, 2021. [2](#)
- [32] J. Xu, S. Liu, A. Vahdat, W. Byeon, X. Wang, and S. De Mello, “Open-vocabulary panoptic segmentation with text-to-image diffusion models,” in *Proceedings of the IEEE/CVF Conference on Computer Vision and Pattern Recognition (CVPR)*, June 2023, pp. 2955–2966. [2](#)
- [33] A. Rahman, J. M. J. Valanarasu, I. Hacihaliloglu, and V. M. Patel, “Ambiguous medical image segmentation using diffusion models,” in *Proceedings of the IEEE/CVF Conference on Computer Vision and Pattern Recognition (CVPR)*, June 2023, pp. 11 536–11 546. [2](#)
- [34] B. Kim, Y. Oh, and J. C. Ye, “Diffusion adversarial representation learning for self-supervised vessel segmentation,” in *Proceedings of the The International Conference on Learning Representations (ICLR)*, 2023. [2](#)
- [35] Y. Ji, Z. Chen, E. Xie, L. Hong, X. Liu, Z. Liu, T. Lu, Z. Li, and P. Luo, “Ddp: Diffusion model for dense visual prediction,” *arXiv preprint arXiv:2303.17559*, 2023. [2](#)
- [36] L. Zbinden, L. Doorenbos, T. Pissas, R. Sznitman, and P. Márquez-Neila, “Stochastic segmentation with conditional categorical diffusion models,” *arXiv preprint arXiv:2303.08888*, 2023. [2](#)
- [37] L. Bogensperger, D. Narnhofer, F. Ilic, and T. Pock, “Score-based generative models for medical image segmentation using signed distance functions,” *arXiv preprint arXiv:2303.05966*, 2023. [2](#)
- [38] T. Chen, C. Wang, and H. Shan, “Berdiff: Conditional bernoulli diffusion model for medical image segmentation,” *arXiv preprint arXiv:2304.04429*, 2023. [2](#)
- [39] J. Wu, “Promptnet: Toward interactive medical image segmentation,” *arXiv preprint arXiv:2305.10300*, 2023. [2](#)
- [40] E. A. Bremping, S. Kornblith, T. Chen, N. Parmar, M. Minderer, and M. Norouzi, “Decoder denoising pretraining for semantic segmentation,” *Transactions of Machine Learning Research*, 2022. [2](#)
- [41] K. Abstreiter, S. Bauer, and A. Mehrjou, “Representation learning in continuous-time score-based generative models,” in *International Conference on Machine Learning (ICML) Workshop*, 2021. [2](#)
- [42] K. Preechakul, N. Chatthee, S. Wizadwongsa, and S. Suwajanakorn, “Diffusion autoencoders: Toward a meaningful and decodable representation,” in *Proceedings of the IEEE Conference on Computer Vision and Pattern Recognition (CVPR)*, 2022, pp. 10 619–10 629. [2](#)
- [43] J. Traub, “Representation learning with diffusion models,” *arXiv preprint arXiv:2210.11058*, 2022. [2](#)
- [44] D. P. Kingma, T. Salimans, B. Poole, and J. Ho, “Variational diffusion models,” in *Proceedings of the Advances in Neural Information Processing Systems (NeurIPS)*, 2021. [2](#)
- [45] Y. Zhu, Y. Wu, K. Olszewski, J. Ren, S. Tulyakov, and Y. Yan, “Discrete contrastive diffusion for cross-modal music and image generation,” in *Proceedings of the The International Conference on Learning Representations (ICLR)*, 2023. [2](#)
- [46] X. Han, H. Zheng, and M. Zhou, “Card: Classification and regression diffusion models,” in *Proceedings of the Advances in Neural Information Processing Systems (NeurIPS)*, 2022. [2](#)
- [47] Y.-C. Cheng, H.-Y. Lee, S. Tulyakov, A. Schwing, and L. Gui, “Sdfusion: Multimodal 3d shape completion, reconstruction, and generation,” *arXiv preprint arXiv:2212.04493*, 2022. [2](#)

- [48] S. Weinbach, M. Bellagente, C. Eichenberg, A. Dai, R. Baldock, S. Nanda, B. Deiseroth, K. Oostermeijer, H. Teufel, and A. F. Cruz-Salinas, “M-vader: A model for diffusion with multimodal context,” *arXiv preprint arXiv:2212.02936*, 2022. [2](#)
- [49] N. Gopalakrishnan Nair, W. Gedara Chaminda Bandara, and V. M. Patel, “Image generation with multimodal priors using denoising diffusion probabilistic models,” *arXiv preprint arXiv:2206.05039*, 2022. [2](#)
- [50] L. Yang, Z. Zhang, Y. Song, S. Hong, R. Xu, Y. Zhao, Y. Shao, W. Zhang, B. Cui, and M.-H. Yang, “Diffusion models: A comprehensive survey of methods and applications,” *arXiv preprint arXiv:2209.00796*, 2022. [2](#)
- [51] K. Q. Weinberger, J. Blitzer, and L. Saul, “Distance metric learning for large margin nearest neighbor classification,” in *Proceedings of the Advances in Neural Information Processing Systems (NeurIPS)*, 2005. [2](#), [4](#)
- [52] G. Chechik, V. Sharma, U. Shalit, and S. Bengio, “Large scale online learning of image similarity through ranking,” *Journal of Machine Learning Research*, vol. 11, no. 3, pp. 1109–1135, 2010. [2](#), [4](#)
- [53] F. Schroff, D. Kalenichenko, and J. Philbin, “Facenet: A unified embedding for face recognition and clustering,” in *Proceedings of the IEEE Conference on Computer Vision and Pattern Recognition (CVPR)*, 2015. [2](#), [4](#)
- [54] K. Sohn, “Improved deep metric learning with multi-class n-pair loss objective,” in *Proceedings of the Advances in Neural Information Processing Systems (NeurIPS)*. Curran Associates, Inc., 2016. [2](#), [4](#)
- [55] T. Chen, S. Kornblith, M. Norouzi, and G. Hinton, “A simple framework for contrastive learning of visual representations,” in *International Conference on Machine Learning (ICML)*, 2020, pp. 1597–1607. [2](#), [3](#), [4](#)
- [56] Z. Xie, Y. Lin, Z. Zhang, Y. Cao, S. Lin, and H. Hu, “Propagate yourself: Exploring pixel-level consistency for unsupervised visual representation learning,” in *Proceedings of the IEEE Conference on Computer Vision and Pattern Recognition (CVPR)*, 2021, pp. 16 684–16 693. [2](#)
- [57] X. Li, Y. Zhou, Y. Zhang, A. Zhang, W. Wang, N. Jiang, H. Wu, and W. Wang, “Dense semantic contrast for self-supervised visual representation learning,” in *Proceedings of the ACM International Conference on Multimedia (ACM MM)*, 2021, pp. 1368–1376. [2](#)
- [58] W. Van Gansbeke, S. Vandenhende, S. Georgoulis, and L. Van Gool, “Unsupervised semantic segmentation by contrasting object mask proposals,” in *Proceedings of the IEEE International Conference on Computer Vision (ICCV)*, 2021, pp. 10 052–10 062. [2](#)
- [59] Z. Wang, Q. Li, G. Zhang, P. Wan, W. Zheng, N. Wang, M. Gong, and T. Liu, “Exploring set similarity for dense self-supervised representation learning,” in *Proceedings of the IEEE Conference on Computer Vision and Pattern Recognition (CVPR)*, June 2022, pp. 16 590–16 599. [2](#)
- [60] W. Wang, T. Zhou, F. Yu, J. Dai, E. Konukoglu, and L. Van Gool, “Exploring cross-image pixel contrast for semantic segmentation,” in *Proceedings of the IEEE International Conference on Computer Vision (ICCV)*, 2021, pp. 7303–7313. [2](#), [3](#)
- [61] X. Wang, H. Zhang, W. Huang, and M. R. Scott, “Cross-batch memory for embedding learning,” in *Proceedings of the IEEE Conference on Computer Vision and Pattern Recognition (CVPR)*, 2020. [3](#)
- [62] X. Chen, H. Fan, R. Girshick, and K. He, “Improved baselines with momentum contrastive learning,” *arXiv preprint arXiv:2003.04297*, 2020. [3](#)
- [63] K. He, H. Fan, Y. Wu, S. Xie, and R. Girshick, “Momentum contrast for unsupervised visual representation learning,” in *Proceedings of the IEEE Conference on Computer Vision and Pattern Recognition (CVPR)*, 2020, pp. 9729–9738. [3](#)
- [64] J. Wang, Z. Zeng, B. Chen, T. Dai, and S.-T. Xia, “Contrastive quantization with code memory for unsupervised image retrieval,” in *Proceedings of the AAAI Conference on Artificial Intelligence (AAAI)*, 2022, pp. 2468–2476. [3](#)
- [65] T. Baltrušaitis, C. Ahuja, and L.-P. Morency, “Multimodal machine learning: A survey and taxonomy,” *IEEE Transactions on Pattern Analysis and Machine Intelligence (T-PAMI)*, vol. 41, no. 2, pp. 423–443, 2018. [3](#)
- [66] B. Kulis, “Metric learning: A survey,” *Found. Trends Mach. Learn.*, vol. 5, no. 4, pp. 287–364, 2013. [Online]. Available: <https://doi.org/10.1561/22000000019> [4](#)
- [67] S. Hershey, S. Chaudhuri, D. P. Ellis, J. F. Gemmeke, A. Jansen, R. C. Moore, M. Plakal, D. Platt, R. A. Saurous, B. Seybold *et al.*, “Cnn architectures for large-scale audio classification,” in *Proceedings of the International Conference on Acoustics, Speech and Signal Processing (ICASSP)*, 2017, pp. 131–135. [5](#)
- [68] J. F. Gemmeke, D. P. Ellis, D. Freedman, A. Jansen, W. Lawrence, R. C. Moore, M. Plakal, and M. Ritter, “Audio set: An ontology and human-labeled dataset for audio events,” in *Proceedings of the International Conference on Acoustics, Speech and Signal Processing (ICASSP)*, 2017, pp. 776–780. [5](#)
- [69] K. He, X. Zhang, S. Ren, and J. Sun, “Deep residual learning for image recognition,” in *Proceedings of the IEEE Conference on Computer Vision and Pattern Recognition (CVPR)*, 2016, pp. 770–778. [5](#)
- [70] W. Wang, E. Xie, X. Li, D.-P. Fan, K. Song, D. Liang, T. Lu, P. Luo, and L. Shao, “Pvt v2: Improved baselines with pyramid vision transformer,” *Computational Visual Media*, vol. 8, no. 3, pp. 415–424, 2022. [5](#)
- [71] A. Kirillov, R. Girshick, K. He, and P. Dollár, “Panoptic feature pyramid networks,” in *Proceedings of the IEEE Conference on Computer Vision and Pattern Recognition (CVPR)*, 2019, pp. 6399–6408. [5](#)
- [72] J. Deng, W. Dong, R. Socher, L.-J. Li, K. Li, and L. Fei-Fei, “Imagenet: A large-scale hierarchical image database,” in *Proceedings of the IEEE Conference on Computer Vision and Pattern Recognition (CVPR)*, 2009, pp. 248–255. [5](#)
- [73] D. P. Kingma and J. Ba, “Adam: a method for stochastic optimization,” in *Proceedings of the The International Conference on Learning Representations (ICLR)*, 2015. [5](#)
- [74] J. Song, C. Meng, and S. Ermon, “Denoising diffusion implicit models,” in *Proceedings of the The International Conference on Learning Representations (ICLR)*, 2020. [6](#)
- [75] Z. Liu, Y. Lin, Y. Cao, H. Hu, Y. Wei, Z. Zhang, S. Lin, and B. Guo, “Swin transformer: Hierarchical vision transformer using shifted windows,” in *Proceedings of the IEEE International Conference on Computer Vision (ICCV)*, 2021, pp. 10 012–10 022. [6](#)
- [76] J. Han, Y. Ren, J. Ding, X. Pan, K. Yan, and G.-S. Xia, “Expanding low-density latent regions for open-set object detection,” in *Proceedings of the IEEE Conference on Computer Vision and Pattern Recognition (CVPR)*, 2022, pp. 9591–9600. [8](#)